

# Opacity modelling of heavy-metal hot subdwarfs. Photoionization of Sr<sup>0</sup>, Y<sup>+</sup> and Zr<sup>2+</sup>.

L. Fernández-Menchero<sup>1\*</sup>, C. S. Jeffery<sup>2</sup>, C. A. Ramsbottom<sup>1</sup> and C. P. Ballance<sup>1</sup>.

<sup>1</sup>Centre of Theoretical Atomic, Molecular and Optical Physics. Queen's University Belfast. University Road, Belfast BT7 1NN.

<sup>2</sup>Armagh Observatory, College Hill, Armagh BT61 9DG.

Accepted XXX. Received YYY; in original form ZZZ

## ABSTRACT

Heavy-metal hot subdwarfs (sdB and sdO) represent a small group of stars with unusually high concentrations of trans-iron elements in their atmospheres, having abundances  $\sim 10000$  times solar. One example is LSIV-14°116, where a number of heavy-metal absorption lines of Sr II, Y III and Zr IV have been observed in the optical band 4000 – 5000 Å. We use a fully relativistic Dirac atomic R-Matrix (DARC) to calculate photoionization cross sections of Sr<sup>0</sup>, Y<sup>+</sup> and Zr<sup>2+</sup> from their ground state to the twentieth excited level. We use the cross sections and the oscillator strengths to simulate the spectrum of a hot subdwarf. We obtain complete sets of photoionization cross sections for the three ions under study. We use these data to calculate the opacity of the stellar atmospheres of hot subdwarf stars, and show that for overabundances observed in some heavy-metal subdwarves, photo-excitation from zirconium, in particular, does contribute some back warming in the model.

**Key words:** Atomic data – photoionization – stars: abundances

## 1 INTRODUCTION

Heavy-metal subdwarfs represent a small fraction of the hot subluminescent stars, O and B stars lying below the main sequence (Heber 2009). The cooler subdwarf B (sdB) stars are low-mass stars with a core of burning helium, and a thinner hydrogen envelope. The majority have masses close to  $0.5M_{\odot}$  and are frequently referred to as ‘extreme horizontal-branch stars’. Owing to competition between gravitational settling and radiative levitation, their photospheres are helium poor and relatively metal-rich (Geier 2013). The hotter subdwarf O stars (sdO) are similar but hotter and, with no hydrogen envelope, the majority lie on or close to the helium main sequence. Their surfaces are mostly hydrogen poor. In between lie a small number of ‘not intermediate helium subdwarfs’, having surface helium-to-hydrogen ratios between 10 and 95% by number (Naslim et al. 2012) and effective temperatures ( $T_{\text{eff}}$ ) between 30000 and 40000 K. Of these, an increasingly large fraction have been discovered to show super-abundances of trans-iron elements forming two groups, the cooler zirconium-rich and the hotter lead-rich *heavy-metal subdwarfs* (Naslim et al. 2011, 2013; Jeffery et al. 2017; Dorsch et al. 2019; Latour et al. 2019; Jeffery & Miszalski 2019; Naslim et al. 2020).

It is well known that under appropriate conditions, radiative levitation can lead to thin layers containing very high concentration of specific ions of heavy atoms in the stellar photosphere (Shulyak et al. 2010). When this concentration occurs at the precise depth at which absorption lines form, abundance measurements return very high values. The line formation depth is closely correlated, for any given ion, with  $T_{\text{eff}}$ , so that in the range of current interest and, specifically in the class prototype, LSIV-14°116, the heavy-metal ions Sr II, Y III and Zr IV, amongst others, were observed with abundances  $\approx 10000$  times solar (Naslim et al. 2011). These abundances are so high that this was the first time some of these ions had been seen in stellar spectra at optical wavelengths, and required the calculation of additional atomic data.

Unfortunately, heavy metals (above Kr) are a largely unexplored field in atomic processes, with the only exceptions being tungsten and molybdenum for their applications in fusion research. Accurate atomic data for the observed lines of heavy elements in dwarf and subdwarf stars are absent in the principal databases. CHIANTI (Del Zanna et al. 2015) contains up-to-date data only for elements up to Zn, OPEN-ADAS<sup>1</sup> includes data of heavy ions only those which are interesting for fusion research, for example tungsten, and

\* E-mail: l.fernandezmenchero@qub.ac.uk (LFM)

<sup>1</sup> <http://open.adas.ac.uk>

the opacity project TOP (Cunto & Mendoza 1992; Cunto et al. 1993; The Opacity Project Team 1995) includes only ions up to iron. In the NIST data base (Kramida et al. 2018), data are only present for level energies, transition wave lengths and ionization potentials for ions of Sr, Y or Zr, and not for transition probabilities, such as line strengths  $S$ , oscillator strengths  $f$ ,  $gf$ , or spontaneous emission  $A$ . Einstein  $A$ -values for transition probabilities for a small set of transitions in the ultraviolet can be found in the Smith et al. (2001) data base for Sr, Y and Zr neutral and once ionized. Radiative and collisional data for these heavy ions are necessary for the correct interpretation of the spectra of metal-rich astrophysical objects. Specifically, data for photoionization and photoexcitation are necessary to construct good models of opacity and atomic diffusion in stellar atmospheres. Data for electron-impact excitation are also necessary in the case of collisional plasmas, in order to construct collisional-radiative models.

Other spectral lines found in these types of stars correspond to the iron-peak elements, Fe III, Fe IV, Ni IV; elements above iron Ga IV, Ge IV, Ge III; and the heavy metal Pb IV. Studies of iron-peak elements have been carried out recently in electron-impact excitation by Smyth et al. (2019a), and photoionisation by Smyth et al. (2018) and Fernández-Menchero et al. (2019). Heavier metals, such as lead, are scarcely explored.

Photoionization of neutral strontium initially in its ground state has been addressed both experimentally and theoretically. Experimentally, Hudson et al. (1969) measured absolute photoionization cross sections for photons with wavelengths between 1646 and 2028 Å, and Brown et al. (1983) between 1400 and 1900 Å. Theoretical studies of photoexcitation were carried out by Aymar (1987) and photoionization by Aymar & Lecomte (1989) using the R-matrix method and the multichannel quantum defect theory (MQDT). More recently, Madine & van der Hart (2005) studied the one- and two-photon ionization of Sr using a time-dependent R-matrix theory in terms of the Floquet approach. They studied the photon-energy ranges from 0.21 to 0.27 a.u. and from 1.105 to 1.158 a.u. and obtained good agreement with the experiments.

For this paper, we calculated the photoionization of neutral Sr and its isoelectronic ions  $Y^+$  and  $Zr^{2+}$ . We also calculated the radiative transition coefficients between all the spectroscopic levels included in the configuration-interaction (CI) expansion of their ionization products:  $Sr^+$ ,  $Y^{2+}$  and  $Zr^{3+}$ . For the scattering calculation, we employ a fully relativistic Dirac Atomic R-matrix Code (DARC), and to obtain the atomic structure of the target, we use the General-purpose Relativistic Atomic Structure Package (GRASP). For the modeling of the stellar atmospheres of the heavy-metal hot subdwarfs, we use the public-use program STERNE (Behara & Jeffery 2006) to obtain the synthetic spectra in a local thermodynamical equilibrium (LTE) approximation.

The paper is organised as follows, in section 2 we describe the atomic structure of the target ions; in section 3 we explain the method used to calculate the photoionization cross sections; in 4 we discuss the most important results for the studied ions; in section 5 we use the calculated data to simulate the spectra of atmospheres of metal-rich hot subdwarf stars in the optical; and finally in section 6 we summarise the most important conclusions of our work. For

a more detailed examination, the complete set of results is provided in the online material. Atomic units are used unless otherwise stated.

## 2 ATOMIC STRUCTURE

To calculate the best quality atomic structure of the target, we use the General-purpose Relativistic Atomic Structure Package (GRASP) (Dyall et al. 1989; Parpia et al. 1996). GRASP uses a multi-configuration Dirac-Fock (MCDF) method to calculate the fully relativistic wave functions of all the atomic levels of the atom or ion in a Coulomb-Dirac framework. The relativistic multi-electron wave function is expanded in terms of a configuration interaction (CI) basis set. The diagonalization of the Dirac-Fock Hamiltonian is carried out through an iterative procedure, until the convergence of the atomic orbitals is reached. One of the problems of the MCDF method concerns convergence, which is often very difficult to achieve. This convergence worsens for lowly charged ions, precisely the ones under investigation in this paper (Froese-Fischer et al. 2007).

We use the same set of configurations in the CI expansion of the three Rb-like ions. We include a total of 34 configurations, including single, double and triple excitations from the ground configurations,  $4p^6 5s$  for  $Sr^+$  and  $Y^{2+}$ , and  $4p^6 4d$  for  $Zr^{2+}$ . For a proper description of the photoionization process initially in excited levels, we also have to include the principal ionization channels of these lower excited configurations of the initial ions:  $4d^2$ ,  $5s^2$ ,  $4d 5s$ ,  $4d 5p$ ,  $5s 5p$ ,  $4d 6s$ ,  $5s 6s$ ,  $5s 6p$ ,  $5p^2$ ,  $5s 4f$ ,  $5s 5d$  (see NIST data tables (Kramida et al. 2018)). We have into take in account in the basis set the ionization of the valence electrons 4d, 5s or above, and the inner electron 4p. From the total of 37 electrons of the target, we freeze 30 of them in the core  $Ar 3d^{10} 4s^2 1S_0^e$ , and the remaining 7 outer electrons, we distribute them in the following set of 34 configurations:

$$\begin{aligned} \text{Even: } & 4p^6 \{4d, 5s, 5d, 6s, 6d\}, \\ & 4p^5 5s \{4f, 5p, 5f, 6p\}, \\ & 4p^5 5p \{4d, 5d, 6s\}, \\ & 4p^5 6s 6p, \\ & 4p^4 \{4d^3, 5s^2 6s\}. \\ \text{Odd: } & 4p^6 \{4f, 5p, 5f, 6p\}, \\ & 4p^5 \{4d^2, 4f^2, 5s^2, 5p^2, 5d^2, 5f^2, 6s^2, 6p^2, 6d^2\}, \\ & 4p^5 5s \{4d, 5d, 6s\}, \\ & 4p^5 5p \{5f, 6p\}, \\ & 4p^4 4f^3. \end{aligned}$$

With this configuration set, we obtain a total of 1615 relativistic levels, 16 of them are spectroscopic, and the rest are energetically above the ionization limit and are embedded in the continuum.

In tables 1 – 3 we compare the calculated theoretical excitation energies of the spectroscopic levels of  $Sr^+$ ,  $Y^{2+}$  and  $Zr^{3+}$  with the observed values tabulated in the NIST atomic spectra data base (Kramida et al. 2018). As expected, we achieve the best agreement with the recommended data for the higher charged ions. For  $Sr^+$ , we reach an agreement below 5% for most of the levels. The most diffuse orbitals, 6d and 5f, have a larger deviation, these orbitals were very difficult to converge in a single-ionized atom.  $Sr^+$  is the only of the three systems with the energy of the 5s orbital below the 4d, in the other two ions, the ground configuration

**Table 1.** Excitation energies of the 16 spectroscopic levels included in the CI expansion of Sr<sup>+</sup>.

<i>i</i>	Configuration	Term	<i>J</i>	parity	GRASP	(%)	NIST
1	4p <sup>6</sup> 5s	<sup>2</sup> S	1/2	even	0.00	–	0.0
2	4p <sup>6</sup> 4d	<sup>2</sup> D	3/2	even	14019.88	–3.7	14555.90
3			5/2	even	14187.46	–4.4	14836.24
4	4p <sup>6</sup> 5p	<sup>2</sup> P <sup>o</sup>	1/2	odd	23459.14	–1.1	23715.19
5			3/2	odd	24232.04	–1.2	24516.65
6	4p <sup>6</sup> 6s	<sup>2</sup> S	1/2	even	48354.77	1.3	47736.53
7	4p <sup>6</sup> 5d	<sup>2</sup> D	3/2	even	53976.98	1.3	53286.31
8			5/2	even	54049.72	1.3	53372.97
9	4p <sup>6</sup> 6p	<sup>2</sup> P <sup>o</sup>	1/2	odd	55677.25	–0.2	55769.7
10			3/2	odd	55943.95	–0.2	56057.9
11	4p <sup>6</sup> 4f	<sup>2</sup> F <sup>o</sup>	7/2	odd	63578.02	4.2	60990.04
12			5/2	odd	63579.81	4.2	60991.34
13	4p <sup>6</sup> 6d	<sup>2</sup> D	3/2	even	78267.46	15.9	67522.87
14			5/2	even	78301.60	15.9	67563.15
15	4p <sup>6</sup> 5f	<sup>2</sup> F <sup>o</sup>	5/2	odd	80150.76	12.8	71065.80
16			7/2	odd	80185.01	12.8	71065.80

Key: *i*: level index; Conf: dominant electron configuration; Term: dominant LS term; *J*: level angular momentum; GRASP: present GRASP calculation; NIST: recommended value from NIST data base (Kramida et al. 2018); %: deviation respect the recommended values of NIST, in percentage. All energies in cm<sup>–1</sup>.

**Table 2.** Excitation energies of the 16 spectroscopic levels included in the CI expansion of Y<sup>2+</sup>.

<i>i</i>	Configuration	Term	<i>J</i>	parity	GRASP	(%)	NIST
1	4p <sup>6</sup> 4d	<sup>2</sup> D	3/2	even	0.00	–	0.0
2			5/2	even	620.63	–14.3	724.15
3	4p <sup>6</sup> 5s	<sup>2</sup> S	1/2	even	9263.19	24.1	7467.1
4	4p <sup>6</sup> 5p	<sup>2</sup> P <sup>o</sup>	1/2	odd	43563.58	5.2	41401.46
5			3/2	odd	45074.35	4.9	42954.87
6	4p <sup>6</sup> 6s	<sup>2</sup> S	1/2	even	89104.89	2.8	86717.59
7	4p <sup>6</sup> 5d	<sup>2</sup> D	3/2	even	91166.57	3.2	88379.61
8			5/2	even	91357.63	3.1	88578.29
9	4p <sup>6</sup> 6p	<sup>2</sup> P <sup>o</sup>	1/2	odd	100977.19	1.6	99345.62
10			3/2	odd	101547.33	1.6	99943.71
11	4p <sup>6</sup> 4f	<sup>2</sup> F <sup>o</sup>	7/2	odd	107933.91	6.8	101088.23
12			5/2	odd	107927.27	6.8	101091.42
13	4p <sup>6</sup> 6d	<sup>2</sup> D	3/2	even	128388.86	7.9	118936.91
14			5/2	even	128489.22	7.9	119029.3
15	4p <sup>6</sup> 5f	<sup>2</sup> F <sup>o</sup>	5/2	odd	131666.08	6.9	123192.92
16			7/2	odd	131728.70	6.1	124193.02

Key: *i*: level index; Conf: dominant electron configuration; Term: dominant LS term; *J*: level angular momentum; GRASP: present GRASP calculation; NIST: recommended value from NIST data base (Kramida et al. 2018); %: deviation respect the recommended values of NIST, in percentage. All energies in cm<sup>–1</sup>.

corresponds to the 4d. For Y<sup>2+</sup>, the deviations are also the order of the 5% except for the most diffuse orbitals 4f, 5f and 6d. In this case, the 4d is the ground configuration and the 5s is very close in energy, with only 7467.1 cm<sup>–1</sup> of energy difference. We conclude that the relative error is small, and artificially increased for these levels. For Zr<sup>3+</sup>, the deviation remains below 5%. As before, the relative error is enhanced for the 4d and 5s levels, but remains small and is less noticeable than in the previous case. We also note the opposite effect for the levels 6d and 5f, in these cases the deviation is larger than for the other orbitals, but the relative error is artificially decreased because the absolute numbers are large.

For a finer check of the quality of the atomic structure,

we compare the radiative transition coefficients, calculated with GRASP in the length and velocity gauges. The ratio between the values calculated with the different gauges should be unitary, fundamentally in the most intense E1 transitions. In tables 4, 5 we show the values of the oscillator strengths *gf* of the transitions present in the optical spectrum of LSIV-14°116. We compare the *gf* values in length and velocity gauges, together with the previous calculations made by Naslim et al. (2011) using the CIV3 code (Hibbert 1975). The ratio between length and velocity gauges for the intense E1 transitions is of the order 1.0 for the Sr<sup>+</sup> and 0.93 for Zr<sup>3+</sup>, and the deviation from the previously calculated values with CIV3 is less than the 10%. From a simulation perspective, for example as input of STERNE and SPECTRUM,

**Table 3.** Excitation energies of the 16 spectroscopic levels included in the CI expansion of  $\text{Zr}^{3+}$ .

$i$	Configuration	Term	$J$	parity	GRASP	(%)	NIST
1	$4p^6 4d$	$^2D$	3/2	even	0.00	–	0.0
2			5/2	even	1173.88	–6.1	1250.7
3	$4p^6 5s$	$^2S$	1/2	even	42045.60	9.9	38258.35
4	$4p^6 5p$	$^2P^o$	1/2	odd	86690.98	5.8	81976.5
5			3/2	odd	89123.42	5.5	84461.35
6	$4p^6 5d$	$^2D$	3/2	even	151566.98	3.4	146652.4
7			5/2	even	151915.60	3.3	147002.46
8	$4p^6 6s$	$^2S$	1/2	even	157000.96	2.9	152513.
9	$4p^6 4f$	$^2F^o$	5/2	odd	168684.56	6.1	159066.75
10			7/2	odd	168740.83	6.1	159086.91
11	$4p^6 6p$	$^2P^o$	1/2	odd	173533.95	2.2	169809.71
12			3/2	odd	174507.06	2.2	170815.11
13	$4p^6 6d$	$^2D$	3/2	even	207260.25	4.8	197765.1
14			5/2	even	207443.08	4.8	197930.43
15	$4p^6 5f$	$^2F^o$	5/2	odd	207759.05	3.3	201114.14
16			7/2	odd	207923.99	3.4	201162.65

Key:  $i$ : level index; Conf: dominant electron configuration; Term: dominant LS term;  $J$ : level angular momentum; GRASP: present GRASP calculation; NIST: recommended value from NIST data base (Kramida et al. 2018); %: deviation respect the recommended values of NIST, in percentage. All energies in  $\text{cm}^{-1}$ .

**Table 4.** Calculated oscillator strengths for transitions in the optical of the ion  $\text{Sr}^+$ .

$i$	$j$	Low lev	Up lev	$\lambda$	$\lambda$ air	$\lambda_{GR}$	GRASP L	GRASP V	$\lambda$ corr	CIV3
1	5	$5s^2 S_{1/2}$	$5p^2 P^o_{3/2}$	4078.86	4077.714	4126.8	1.44	1.44	1.46	1.39
1	4	$5s^2 S_{1/2}$	$5p^2 P^o_{1/2}$	4216.71	4215.524	4262.7	0.698	0.698	0.706	0.668

Key:  $i$ : lower level index;  $j$ : upper level index;  $\lambda$ : transition wavelength in  $\text{\AA}$ , observed in vacuum;  $\lambda$  air: transition wavelength in  $\text{\AA}$ , observed in air;  $\lambda_{GR}$ : transition wavelength in  $\text{\AA}$ , calculated with GRASP; GRASP L:  $gf$  value calculated with GRASP in length gauge; GRASP V: idem in velocity gauge;  $\lambda$  corr:  $gf$  in length gauge corrected the wavelength with the observed value; CIV3:  $gf$  value calculated with CIV3 in reference (Naslim et al. 2011).

**Table 5.** Calculated oscillator strengths for transitions in the optical of the ion  $\text{Zr}^{3+}$ .

$i$	$j$	Low lev	Up lev	$\lambda$	$\lambda$ air	$\lambda_{GR}$	GRASP L	GRASP V	$\lambda$ corr	CIV3
6	12	$5d^2 D_{3/2}$	$6p^2 P^o_{3/2}$	4138.6	4137.435	4359.2	0.243	0.226	0.256	0.237
7	12	$5d^2 D_{5/2}$	$6p^2 P^o_{3/2}$	4199.4	4198.265	4426.5	2.19	2.04	2.31	2.10
6	11	$5d^2 D_{3/2}$	$6p^2 P^o_{1/2}$	4318.3	4317.081	4552.3	1.20	1.13	1.27	1.17

Key:  $i$ : lower level index;  $j$ : upper level index;  $\lambda$ : transition wavelength in  $\text{\AA}$ , observed in vacuum;  $\lambda$  air: transition wavelength in  $\text{\AA}$ , observed in air;  $\lambda_{GR}$ : transition wavelength in  $\text{\AA}$ , calculated with GRASP; GRASP L:  $gf$  value calculated with GRASP in length gauge; GRASP V: idem in velocity gauge;  $\lambda$  corr:  $gf$  in length gauge corrected the wavelength with the observed value; CIV3:  $gf$  value calculated with CIV3 in reference (Naslim et al. 2011).

it is better to employ modified oscillator strengths that have incorporated the NIST observed energy values for the atomic structure. In tables we also show this corrected values of  $gf$ , its variation is quite small, below the 10%.

For the online material, we provide the complete table for the radiative transition coefficients E1, M1, E2 and M2 obtained with GRASP between all the spectroscopic levels of the targets  $\text{Sr}^+$ ,  $\text{Y}^{2+}$  and  $\text{Zr}^{3+}$ .

### 3 SCATTERING

We use a fully relativistic Dirac atomic R-matrix code (DARC) (Ait-Tahar et al. 1996; Norrington & Grant 1981, 1987) to calculate the photoionization cross sections of Sr,  $\text{Y}^+$  and  $\text{Zr}^{2+}$  initially in their ground or excited levels. In the inner region, we employ the dipole version of the DARC package, including the recent upgrades to optimise the usage of memory and processor load balancing using the MPI protocol Ballance & Griffin (2004); Smyth et al. (2019b).

In the outer region, we use the community code PST-GBF0DAMP (Gorczyca and Badnell, unpublished). PST-GBF0DAMP calculates bound-continuum transitions in the

$N+1$ -electron atom, produced by photon absorption. In consequence, apart from the Hamiltonian matrixes for each  $J\pi$  symmetry, we need to calculate with DARC the dipole matrixes between the possible pairs of E1-connected symmetries. We have also to calculate the bound states of each symmetry of the  $N+1$ -electron system. For that goal, we use the STGB program Seaton (1982); Berrington et al. (1987). STGB was recently upgraded by our group, we implemented a CUDA-FORTRAN environment to take advantage of the modern GPU-based architectures. This upgrade reduced the computation time up to a factor 20 in some cases. Finally, we use the bound-bound program STGBB to calculate the electric dipole photoexcitation transition coefficients of the  $N+1$ -electron atom.

To run PSTGBF0DAMP, we split the photon-energy grid in two different sets. Firstly, a fine mesh in order to map the narrow resonances at low energies. This set contains at least the electron final energies up to the last spectroscopic level included in the CC expansion. In this section, we fix the energy mesh to a fine value of  $10^{-5}z^2$  Ry, with  $z$  the final ion charge. The second set is above the final level included within the close-coupling expansion, above which we expect no fine resonance structure, so we can set a coarser mesh. This section extends from the end of the previous fine mesh up to approximately two times the second ionization threshold, this upper limit is far enough to model opacities of photoionized plasmas at temperatures of the order of 40 000 K. We fix this coarse energy mesh to  $10^{-3}z^2$  Ry. Above the limit of double-ionization, additional processes should be taken into account, such as Auger autoionization. This processes can affect the resonance structure of the cross sections, but not to the background. With the present method, we can calculate with good accuracy photoionization cross sections for photon energy up to at least 6 Ry in the Sr atom, 8 Ry in the Y<sup>+</sup> and 10 Ry in the Zr<sup>2+</sup>, which is more than enough to model the opacity in the optical band of the spectrum of LS IV-14°116 or other hot subdwarf stars.

We include in the close-coupling (CC) expansion enough levels to make sure we have no pseudoresonances in a wide enough range of photon energies. For the three ions we include a total of 300 levels in the CC expansion of the total of 1615 calculated in the CI calculation. Then we are sure we have cross sections free of pseudoresonances for ejected-electron energies lower than 2.38 Ry for the Sr, 2.68 Ry for the Y<sup>+</sup> and 3.71 Ry for the Zr<sup>2+</sup>. We also review all the calculated cross sections to double check if pseudoresonances are present at energies above these maxima. To have a good description of the ionization continuum in the whole range of calculated photon energies we include a total of 36 continuum functions in the case of Sr, 30 for Y<sup>+</sup>, and 26 for Zr<sup>2+</sup>.

We calculate the photoionization of each parent ion initially in its ground level and excited levels up to approximately the 20th. All these initial levels are contained in the symmetries with initial angular momenta  $J = 0-4$  and both parities. The maximum number of channels in a symmetry is 1604 for the Sr, 1608 for the Y<sup>+</sup>, and 1667 for the Zr<sup>2+</sup>.

The atmosphere of LS IV-14°116 is a photoionized plasma, and the temperature of the chromosphere of the star is of 34 000 K, equivalent to 0.22 Ry. In this case, photoionization cross sections with photon energies up to the second ionization potential of Sr, Y<sup>+</sup> and Zr<sup>2+</sup> constitute a complete

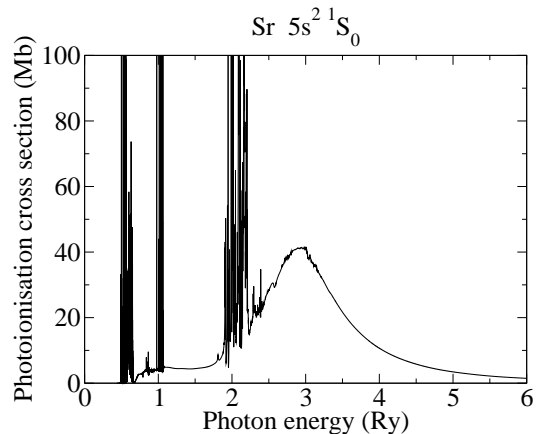


**Figure 1.** Photoionization cross section of Sr initially in its ground level versus photon energy.

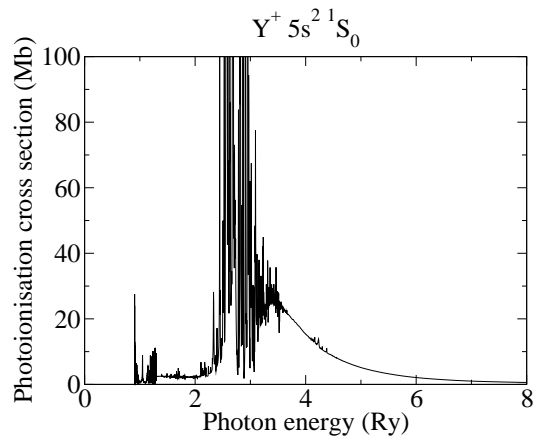


**Figure 2.** Photoionization cross section of Y<sup>+</sup> initially in its ground level versus photon energy.

enough data set to construct a good opacity model. These calculated cross sections also fit for the modelling of other subdwarf stars SdA and SdO, as all of them have surface temperatures in this range.

## 4 RESULTS

In figures 1 – 3, we show the calculated photoionization cross sections of Sr, Y<sup>+</sup> and Zr<sup>2+</sup> initially in their ground level. We get the usual structure of a photoionization cross section, of resonances superimposed over a background. The background shows two big increases with posterior decays, these big growths correspond to the ionization of an individual orbital, the first one of the outer electron, 4d or 5s, and the second, one of the inner electron 4p. For the lower-charged ions, Sr and Y<sup>+</sup>, the ground configuration is the 5s<sup>2</sup>. As the charge increases, the relative energy of the 4d orbital reduces, and for Zr<sup>2+</sup> it positions below the 5s. In consequence, the ground configuration of Zr<sup>2+</sup> changes to the 4d<sup>2</sup>, in opposition to the other two ions. The photoionization cross section from the ground level of Zr<sup>2+</sup> has a slightly different

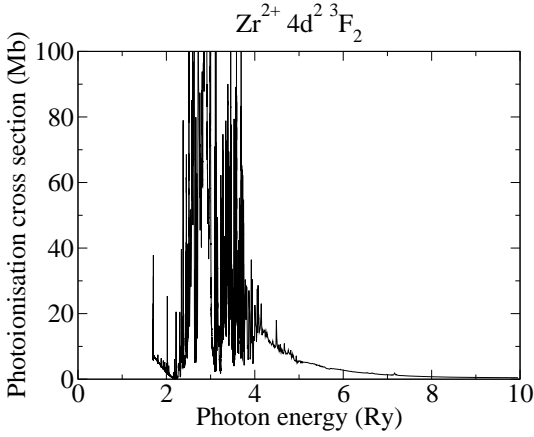


**Figure 3.** Photoionization cross section of  $\text{Zr}^{2+}$  initially in its ground level versus photon energy.

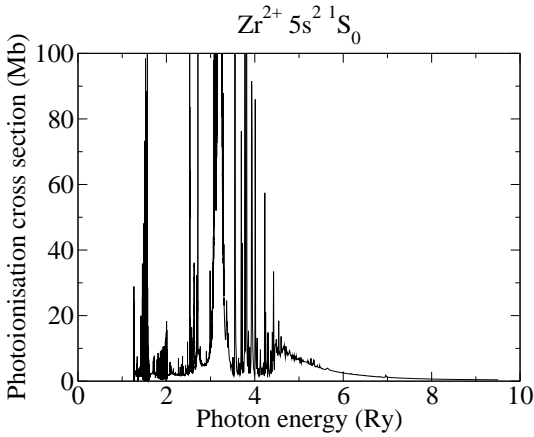


**Figure 4.** Photoionization cross section of  $\text{Zr}^{2+}$  initially in the excited level  $5s^2 1S_0$  versus photon energy.

behaviour with respect to the other two ions, in particular at photon energies below the second threshold, when the ionized electron is the 4d instead of the 5s. For the ionization from the 4d, the value of the cross section just above the threshold is not zero. For higher energies, above the ionization threshold of the inner 4p electron, the background of the cross section is similar for the three ions. For comparison with the ground state of the other two ions, we show in figure 4 the photoionization cross section of  $\text{Zr}^{2+}$  initially in the excited level  $5s^2 1S_0$ . In this case, the cross section starts at zero just above the threshold.

For the online material we provide the complete set of photoionization cross sections from ground and excited levels of Sr,  $\text{Y}^+$ , and  $\text{Zr}^{2+}$  in TOP format (The Opacity Project Team 1995), and the complete set of bound-bound photoexcitation transition coefficients for all the electric-dipole allowed transitions within the same set of levels for these three parent ions. To ensure the files maintain a reasonable downloadable size, order megabytes, we convoluted the cross sections to reduce their size to around one thousand points in each initial level. The complete photoionization cross sec-

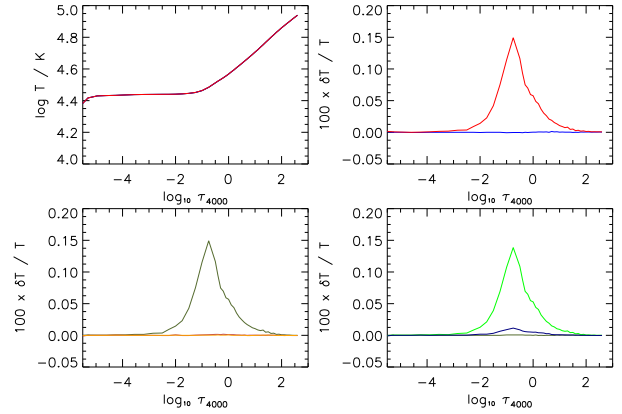


**Figure 5.** The temperature structure of model atmospheres with a 20000-fold (+4.3 dex) enhancement of one or more of the s-process elements strontium, yttrium and germanium are compared with a model having a near-solar abundance of the same elements. All models have  $T_{\text{eff}} = 34\,000$  K,  $\log g / \text{cm s}^{-2} = 5.5$  and other properties as shown in table 6. All panels are plotted as functions of monochromatic optical depth  $\tau_{4000}$ . Trans-iron ions included are:  $\text{Sr}^0$ ,  $\text{Sr}^+$ ,  $\text{Y}^+$ ,  $\text{Y}^{2+}$ ,  $\text{Zr}^{2+}$ ,  $\text{Zr}^{3+}$ . Top left: temperature structure  $T / (\text{K})$  for both the reference model (near solar abundances of Sr, Y and Zr) and the final model (Sr, Y and Zr abundances increased by +4.3 dex); top right: relative difference ( $\delta T / T$  per cent) between models with normal and +4.3 dex enhanced abundances of Sr, Y and Zr contributing to a) photo-ionization only (blue), and b) photo-ionisation and photo-excitation combined (red); bottom left: relative difference between models with and without photo-excitation showing the contributions of Sr (orange), Y (maroon) and Z (olive) separately; bottom right: relative difference between models with and without photo-excitation showing the contributions of no photo-excitation (olive),  $\text{Zr}^{2+}$  (green) and  $\text{Zr}^{3+}$  (blue) photo-excitation separately.

**Table 6.** Model atmosphere parameters for LS IV-14 $^{\circ}$ 116

$T_{\text{eff}} / \text{K}$	34000	
$\log g / \text{cm s}^{-2}$	5.5	
$v_{\text{turb}} / \text{km s}^{-1}$	5	
$\frac{n_{\text{H}}}{n}$	0.64	
$\frac{n_{\text{He}}}{n}$	0.32	
$\frac{n_{\text{C}}}{n}$	0.014	
$\frac{n_{\text{N}}}{n}$	0.014	
[O]	-0.8	
[Si]	-0.8	
[Ca]	-0.25	$Z = 17 - 25$
[Fe]	-0.55	$Z \geq 26$
[Sr]	-0.25 +4.05	
[Y]	-0.25 +4.05	
[Zr]	-0.25 +4.05	

tions, without any convolution, are available for any user under request. These cross sections can be used for modelling the opacity of astrophysical objects, such as stellar atmospheres.

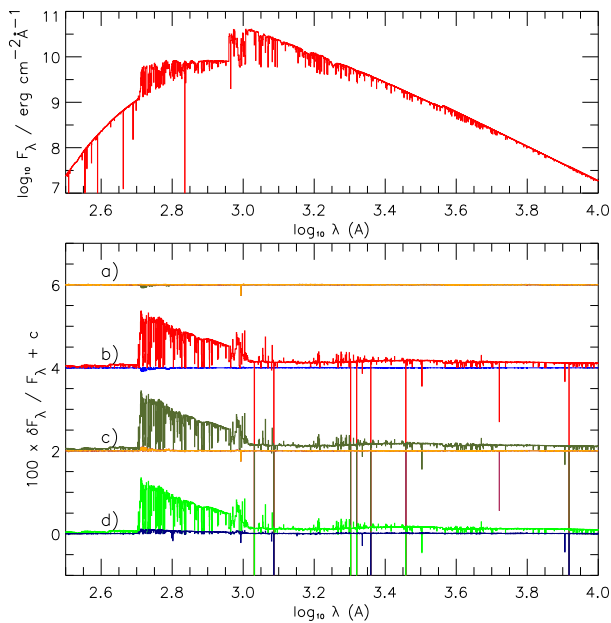


**Figure 6.** The flux emergent from model atmospheres shown in Fig. 5. All panels are plotted as functions of wavelength  $\log \lambda / (\text{\AA})$  with  $300 \text{\AA} < \lambda < 10000 \text{\AA}$ . Top: The overall flux distribution for the final model including photo-ionisation and photo-excitation of Sr, Y and Zr enhanced by +4.3 dex; bottom: a) (displaced by +6%) relative difference between models with Sr (orange), Y (maroon) and Zr (olive) enhanced individually by +4.3 dex and with no enhancement, including photo-ionisation only (all models are essentially indistinguishable); b) (+4%) relative difference between models with Sr, Y and Zr enhanced collectively by +4.3 dex and with no enhancement, and including photo-ionisation only (blue) and also photo-excitation (red). c) (+2%) relative difference between models with and without photo-excitation showing the contributions of Sr (orange), Y (maroon) and Zr (olive) separately (Sr and Y are indistinguishable); d) relative difference between models with and without photo-excitation showing the contributions of Zr<sup>2+</sup> (green) and Zr<sup>3+</sup> (blue) photo-excitation separately. Zr<sup>2+</sup> lines provide the major opacity source.

## 5 MODELLING OF STELLAR ATMOSPHERE

Using STERNE, we calculated models for the atmosphere of LSIV-14°116 assuming base parameters given in Table 6 for effective temperature  $T_{\text{eff}}$ , surface gravity  $g$ , microturbulent velocity  $v_{\text{turb}}$ , fractional abundances by number for hydrogen, helium, carbon and nitrogen  $n_i$ , and logarithmic abundances of heavier species relative to solar  $[X] \equiv \log \frac{n_X}{n_{X\odot}}$ . For Sr, Y and Zr, we used two values, one being scaled to the light metals Ca – Mn (the reference model), and the second enhanced by a factor 20 000 (+4.3 dex), the latter corresponds approximately to the overabundances observed in LSIV-14°116.

We construct ten different models in three groups. All models include the photoionisation cross-sections calculated here for Sr<sup>0</sup>, Y<sup>+</sup> and Zr<sup>2+</sup>. The reference model has no enhancement in the abundances of these elements. There are four models which include abundances of Sr, Y, and Zr enhanced by +4.3 dex, each individually and all collectively. The third group of models includes a revised linelist with the calculated photo excitation transitions of the parent ions Sr<sup>0</sup>, Y<sup>+</sup>, Zr<sup>2+</sup>, and the ionization products Sr<sup>+</sup>, Y<sup>2+</sup>, Zr<sup>3+</sup>. Again

Sr, Y, and Zr are enhanced by +4.3 dex, individually and collectively. In addition, two models were computed with the Zr<sup>2+</sup> and Zr<sup>3+</sup> lines included separately.

Figure 5 (top left) shows the temperature structure of model atmospheres  $T$  versus optical depth  $\tau_{4000}$  for different abundances of Sr, Y and Zr. Remaining panels show the temperature relative difference (per cent) to the reference model for various cases. Results imply that the new photo-ionisation cross section makes negligible difference to the total opacity, even with the high abundances adopted. The photo-excitation transitions make a modest temperature difference in the line-forming region ( $0.01 < \tau_{4000} < 1$ ), but only due to a number of very strong Zr lines. This difference corresponds to a temperature increase of up to 0.15%.

The consequences for the overall flux distribution are also modest and are illustrated in figure 6, where the emergent fluxes  $F_\lambda$  ( $\text{erg cm}^{-2} \text{\AA}^{-1}$ ) (top) and differences relative to the reference model (middle and bottom) are shown as a function of wavelength  $\lambda$  ( $\text{\AA}$ ). Again, only the inclusion of the photo-excitation process for Zr ions significantly disturbs the flux distribution, indicating substantial flux blocking by these ions.

## 6 CONCLUSIONS

We present high-quality photoionization cross sections of Sr, Y<sup>+</sup>, and Zr<sup>2+</sup>, initially in their ground and excited levels. We present also the bound-bound photoexcitation transition coefficients for the same three ions and their ionization products Sr<sup>+</sup>, Y<sup>2+</sup>, and Zr<sup>3+</sup>. We calculate all the symmetries with total angular momentum  $J = 0 - 4$  and both parities. With the set of configurations included in the basis set, we are able to calculate the cross sections from the initial level up to the twentieth excited.

We include a basis set of 34 non-relativistic interacting configurations to get the structure of the targets Sr<sup>+</sup>, Y<sup>2+</sup>, and Zr<sup>3+</sup>. We get accurate energies and transition coefficients for all the first 16 spectroscopic levels.

The results of photoionization and photoexcitation are available to be used for modelling the opacities of astrophysical objects. The transition coefficients, such as the oscillator strengths, to model the absorption spectral lines, and to build synthetic spectra. These synthetic spectra can be compared with observed ones to determine physical parameters of the astrophysical objects, for example chemical abundances of the elements.

In particular, we have used the model atmosphere program STERNE to test the contribution of these new data to the atmospheres of hot subdwarf stars. We compare the differences in the models taking into account only the photoionization cross sections, and including also the photoexcitation transitions. We find that the photo-excitation transitions, from Zr ions in particular, contribute significant back warming in the model atmosphere model when this element is substantially overabundant, as observed in the heavy-metal subdwarf LSIV-14°116.

Complete sets of photoionization cross sections and radiative coefficients are provided in the online material. Results will be uploaded to the web page of the Opacity

Project<sup>2</sup> for public use. Due to the large size of the files, photoionization cross sections were reduced using a convolution, the complete set is available under request.

## ACKNOWLEDGMENTS

Present work has been funded by the STFC through the QUB Astronomy Observation and Theory Consolidated Grant ST/P000312/1. The computation has been performed in the supercomputer Archer, property of the Engineering and Physical Science Research Council under the allocation E585-AMOR.

## REFERENCES

- Ait-Tahar S., Grant I. P., Norrington P. H., 1996, *Phys. Rev. A*, 54, 3984
- Aymar M., 1987, *J. Phys. B: At. Mol. Phys.*, 20, 6507
- Aymar M., Lecomte J. M., 1989, *J. Phys. B: At. Mol. Opt. Phys.*, 22, 223
- Ballance C. P., Griffin D. C., 2004, *J. Phys. B*, 37, 2943
- Behara N. T., Jeffery C. S., 2006, *Astron. Astroph.*, 451, 643
- Berrington K. A., Burke P. G., Butler K., Seaton M. J., Storey P. J., Taylor K. T., Yan Y., 1987, *J. Phys. B: At. Mol. Phys.*, 20, 6379
- Brown C. M., Longmire M. S., Ginter M. L., 1983, *J. Opt. Soc. Am.*, 73, 985
- Cunto W., Mendoza V., 1992, *Rev. Mexicana Astron. Astrofis.*, 23, 107
- Cunto W., Mendoza C., Ochsenein F., Zeppen C. J., 1993, *Astron. Astroph.*, 275, L5
- Del Zanna G., Dere K. P., Young P. R., Landi E., Mason H. E., 2015, *Astron. Astroph.*, 582, A56
- Dorsch M., Latour M., Heber U., 2019, *Astron. Astroph.*, 630, A130
- Dyall K. G., Grant I. P., Johnson C. T., Parpia F. A., Plummer E. P., 1989, *Comp. Phys. Comm.*, 55, 425
- Fernández-Menchero L., Smyth R. T., Ramsbottom C. A., Ballance C. P., 2019, *Mon. Not. R. Astr. Soc.*, 483, 2154
- Froese-Fischer C., Tachiev G., Gaigalas G., Godefroid M. R., 2007, *Comp. Phys. Comm.*, 176, 559
- Geier S., 2013, *Astron. Astroph.*, 549, A110
- Heber U., 2009, *Ann. Rev. Astron. Astroph.*, 47, 211
- Hibbert A., 1975, *Comp. Phys. Comm.*, 9, 141
- Hudson R. D., Carter V. L., Young P. A., 1969, *Phys. Rev.*, 180, 77
- Jeffery C. S., Miszalski B., 2019, *Mon. Not. R. Astr. Soc.*, 489, 1481
- Jeffery C. S., et al., 2017, *Mon. Not. R. Astr. Soc.*, 465, 3101
- Kramida A., Yu. Ralchenko Reader J., and NIST ASD Team 2018, NIST Atomic Spectra Database (ver. 5.5.6), [Online]. Available: <https://physics.nist.gov/asd> [2018, June 27]. National Institute of Standards and Technology, Gaithersburg, MD.
- Latour M., Dorsch M., Heber U., 2019, *Astron. Astroph.*, 629, A148
- Madine M., van der Hart H. W., 2005, *J. Phys. B: At. Mol. Opt. Phys.*, 38, 1895
- Naslim N., Jeffery C. S., Behara N. T., Hibbert A., 2011, *Mon. Not. R. Astr. Soc.*, 412, 363
- Naslim N., Geier S., Jeffery C. S., Behara N. T., Woolf V. M., Classen L., 2012, *Mon. Not. R. Astr. Soc.*, 423, 3031
- Naslim N., Jeffery C. S., Hibbert A., Behara N. T., 2013, *Mon. Not. R. Astr. Soc.*, 434, 1920
- Naslim N., Jeffery C. S., Woolf V. M., 2020, *Mon. Not. R. Astr. Soc.*, 491, 874
- Norrington P. H., Grant I. P., 1981, *J. Phys. B: At. Mol. Phys.*, 14, L261
- Norrington P. H., Grant I. P., 1987, *J. Phys. B: At. Mol. Opt. Phys.*, 20, 4869
- Parpia F. A., Fischer C. F., Grant I. P., 1996, *Comp. Phys. Comm.*, 94, 249
- Seaton M., 1982, *Comp. Phys. Comm.*, 25, 87
- Shulyak D., Ryabchikova T., Kildiyarova R., Kochukhov O., 2010, *Astron. Astroph.*, 520, A88
- Smith P. L., Heise C., Esmond J. R., Kurucz R. L., 2001, <https://www.cfa.harvard.edu/amp/ampdata/kurucz23/sekur.html>
- Smyth R. T., Ramsbottom C. A., Ballance C. P., 2018, *Mon. Not. R. Astr. Soc.*, p. submitted
- Smyth R. T., Ramsbottom C. A., Keenan F. P., Ferland G. J., Ballance C. P., 2019a, *Mon. Not. R. Astr. Soc.*, 483, 654
- Smyth R. T., Ballance C. P., Ramsbottom C. A., 2019b, *The Astrophysical Journal*, 874, 144
- The Opacity Project Team 1995, *The Opacity Project Vol. 1*. Institute of Physics Publications, Bristol, UK

This paper has been typeset from a  $\text{\TeX}/\text{\LaTeX}$  file prepared by the author.

<sup>2</sup> <http://op-opacity.obspm.fr/opacity/>